AIAA 2012–4585

Impulsive Feedback Control of Non-singular Elements in the Geostationary Regime

Paul V. Anderson and Hanspeter Schaub

University of Colorado, Boulder, CO, 80309, USA

AIAA Astrodynamics Specialist Conference
August 13–16, 2012 / Minneapolis, MN

Impulsive Feedback Control of Nonsingular Elements in the Geostationary Regime

Paul V. Anderson* and Hanspeter Schaub†
University of Colorado, Boulder, CO, 80309, USA

An N-impulse feedback control strategy is developed to mitigate specified errors in a set of nonsingular orbit element differences between a chief and deputy craft. While suitable for general orbits, this strategy is motivated by relative control in the geosynchronous regime. The linear mapping between these nonsingular element differences and the Hill frame state of the deputy is derived, and the Gaussian variational equations for the nonsingular set are developed as a basis for the fuel-optimal control strategy. Three examples demonstrate that this method is proficient in detecting Δv-optimal burn locations for general orbit transfers.

I Introduction

SPACECRAFT formation flying is a challenging problem that has been broadly studied in the literature,[1,2,3] and with renewed interest in on-orbit servicing and refueling applications, the problems of relative motion and intersatellite rendezvous, especially in the geostationary (GEO) regime, take on renewed importance.[4,5,6] Conventional orbit propagation and estimation employ classical Keplerian elements or Cartesian position and velocity to characterize state, but these representations are not ideal for near-geostationary motion: classical elements are not well-defined for weakly-eccentric and weakly-inclined orbits typical of the GEO regime, and rapidly-changing Cartesian coordinates mask the near-linearity of geosynchronous motion.[7] Nonsingular sets are thus desirable for describing motion near the GEO altitude. This study implements an element difference description[2] of relative motion, using the nonsingular set $\boldsymbol{e} \equiv (a, \xi, \eta, \zeta, \psi, \lambda)$, where a is the semi-major axis of the orbit and the other parameters are defined by:[8]

$$\begin{aligned} \xi &\equiv e\sin(\omega+\Omega) \\ \eta &\equiv e\cos(\omega+\Omega) \\ \zeta &\equiv \sin(i/2)\sin(\Omega) \\ \psi &\equiv \sin(i/2)\cos(\Omega) \\ \lambda &\equiv f+\omega+\Omega \end{aligned} \tag{1}$$

The classical Keplerian elements of eccentricity e, inclination i, right ascension of ascending node Ω, argument of periapsis ω, and true anomaly f are thereby used to assemble the nonsingular set presented in Equation (1). The inertial Cartesian state of the chief and deputy satellites may be readily mapped to the classical set, which is thereafter transformed to the nonsingular set with the above formulation. Note that this nonsingular set is a modified variant of the equinoctial element set established by Broucke,[9] in which the $\tan(i/2)$ factor inherent to the ζ and ψ elements has been replaced with a $\sin(i/2)$ factor to eliminate the singularity occurring at the retrograde inclination $i = 180°$. The nonsingular set $\boldsymbol{e}$ furthermore differs from the conventional equinoctial set by implementing the true anomaly f (instead of the mean anomaly) in the definition of the true longitude parameter λ, in order to simplify the derivations detailed in Sections II-III. The modified elements presented in Equation (1) are valid for zero eccentricity and inclination, and are thereby well-defined for the description of relative motion in the geostationary regime.

This study presents the forward linear mapping that transforms the nonsingular element difference vector $\delta\boldsymbol{e} = \boldsymbol{e}_d - \boldsymbol{e}_c$, where $\boldsymbol{e}_d$ and $\boldsymbol{e}_c$ denote the elements of the deputy and chief satellites, respectively, into the relative Cartesian state of the deputy object as observed by the chief satellite in the Hill frame of reference.[10] Furthermore, the nonconservative variational equations for the nonsingular set are derived, and implemented as the foundation for an impulsive

*Graduate Student, Department of Aerospace Engineering Sciences, 429 UCB, Boulder, CO, 80309. AIAA Student Member.
†Associate Professor, Associate Chair of Graduate Affairs, Department of Aerospace Engineering Sciences, 429 UCB, Boulder, CO, 80309. AIAA Associate Member.

feedback control scheme that seeks to efficiently minimize fuel expenditures for formation maintenance applications, or more generally, solutions to the optimal orbit correction problem.

Impulsive feedback control methodology has been extensively studied in the literature,[1,11,12,13] but many of these methods rely upon complicated, time-consuming optimization algorithms to determine fuel-optimal burn placement.[14,15] In a general orbit correction problem, the initial conditions for an optimization routine are non-intuitive and difficult to discern – to alleviate this issue, this study presents a fuel-optimal, time-fixed N-impulse method to determine appropriate initial conditions for more complicated trajectory optimization routines, with minimal computing time. This N-impulse technique solves a simple fuel-minimization problem subject to linear constraints, to rapidly "detect" locations at which corrective impulses should be performed.

II Development of Forward Linear Mapping

Analytic derivation of the forward linear mapping from differences in the nonsingular orbital element set provided in Equation (1) to the corresponding Hill frame Cartesian state $(x, y, z, \dot{x}, \dot{y}, \dot{z})^T$ of the deputy object is performed by transforming the appropriate variational terms in the linear mapping developed in Alfriend.[16] The noninertial Hill frame of reference is centered at the chief spacecraft of interest and implements rotating axes that point in the local radial ($\hat{\boldsymbol{o}}_r$), in-track ($\hat{\boldsymbol{o}}_i$), and cross-track ($\hat{\boldsymbol{o}}_c$) directions of the chief spacecraft.[10] For reference, the Hill frame description of relative motion is illustrated within Figure 1. The linear mapping

$$\boldsymbol{X} = [A(\boldsymbol{e}_c)]\delta\boldsymbol{e} \tag{2}$$

wherein the Hill frame state $\boldsymbol{X} = (x, y, z, \dot{x}, \dot{y}, \dot{z})^T$ is thus converted into a form consistent with the description

$$\delta\boldsymbol{e} = \boldsymbol{e}_d - \boldsymbol{e}_c \equiv (\delta a, \delta\xi, \delta\eta, \delta\zeta, \delta\psi, \delta\lambda)^T \tag{3}$$

for relative deputy orbits that are *small*[a] as compared with the chief orbit radius.[10] Note that although this formulation facilitates perturbations, Keplerian motion is henceforth assumed for the purposes of this study; each of the nonsingular orbit element differences with the exception of $\delta\lambda$ are invariant in this two-body case.

II.A Mapping to Hill Frame Position

Relative Hill frame Cartesian position $(x, y, z)^T$ is expressed in terms of classical orbital element differences as:[16]

$$x = \delta r \tag{4}$$

$$y = r(\delta\theta + \cos i\, \delta\Omega) \tag{5}$$

$$z = r(\sin\theta\, \delta i - \cos\theta \sin i\, \delta\Omega) \tag{6}$$

where r, i, and θ are the chief orbit radius, inclination, and argument of latitude ($\theta = \omega + f$), respectively. Formulating the conic equation in terms of the nonsingular orbit element set, the orbit radius is cast:

$$r = \frac{a\left(1 - \xi^2 - \eta^2\right)}{1 + \eta\cos\lambda + \xi\sin\lambda} \tag{7}$$

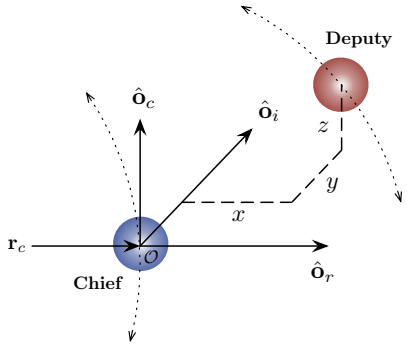

Figure 1: Hill relative motion frame.

The first variation of the chief radius r is therefore expressed as

$$\delta r = \frac{r}{a}\delta a - \frac{r}{p}(2a\xi + r\sin\lambda)\,\delta\xi - \frac{r}{p}(2a\eta + r\cos\lambda)\,\delta\eta + r\left(\frac{V_r}{V_t}\right)\delta\lambda \tag{8}$$

where V_r and V_t are the radial and transverse velocity components of the chief craft, defined by

$$V_r = \frac{h}{p}(\eta\sin\lambda - \xi\cos\lambda) \tag{9}$$

$$V_t = \frac{h}{p}(1 + \eta\cos\lambda + \xi\sin\lambda) \tag{10}$$

[a]The forward mapping implements linearization about the chief orbital motion – deviation from this reference must therefore be *small* such that this linear approximation remains valid in the truncation of higher-order terms beyond those of the first-order.

where h and p denote the specific angular momentum and semi-latus rectum of the chief's orbit, respectively. Defining $\alpha \equiv a/r$, $\rho \equiv r/p$, and $\nu \equiv V_r/V_t$ for simplicity,[10] substituting Equation (8) into Equation (4) yields:

$$x = \frac{1}{\alpha}\delta a - \rho\left(2a\xi + r\sin\lambda\right)\delta\xi - \rho\left(2a\eta + r\cos\lambda\right)\delta\eta + r\nu\delta\lambda \tag{11}$$

For transformation of Equation (5), note that the right ascension of the ascending node of the chief spacecraft is uniquely determined with $\Omega = \tan^{-1}(\zeta/\psi)$. The first variation of this parameter is therefore expressed as:

$$\delta\Omega = \frac{\psi}{\zeta^2+\psi^2}\delta\zeta - \frac{\zeta}{\zeta^2+\psi^2}\delta\psi \tag{12}$$

Considering the nonsingular element $\lambda = f + \omega + \Omega = \theta + \Omega$, the first variation of the argument of latitude is

$$\delta\theta = -\frac{\psi}{\zeta^2+\psi^2}\delta\zeta + \frac{\zeta}{\zeta^2+\psi^2}\delta\psi + \delta\lambda \tag{13}$$

Noting that $\zeta^2 + \psi^2 = \sin^2(i/2)$, it is readily shown that $\cos i = 1 - 2\zeta^2 - 2\psi^2$. Substituting into Equation (5) with Equations (49), (12), and (13), the Cartesian in-track component of position may be expressed as follows:

$$y = r\left(-2\psi\delta\zeta + 2\zeta\delta\psi + \delta\lambda\right) \tag{14}$$

Conversion of Equation (6) requires trigonometric development of intermediate results. Recalling $\theta = \lambda - \Omega$:

$$\cos\theta = \cos\lambda\cos\Omega + \sin\lambda\sin\Omega \tag{15a}$$
$$\sin(i/2)\cos\theta = \psi\cos\lambda + \zeta\sin\lambda \tag{15b}$$
$$2\cos(i/2)\sin(i/2)\cos\theta = 2\cos(i/2)\left(\psi\cos\lambda + \zeta\sin\lambda\right) \tag{15c}$$
$$\sin i\cos\theta = 2\cos(i/2)\left(\psi\cos\lambda + \zeta\sin\lambda\right) \tag{15d}$$

Employing the relation $\zeta^2 + \psi^2 = \sin^2(i/2)$, it may be demonstrated that $\cos(i/2) = \sqrt{1-\zeta^2-\psi^2}$. Thereby:

$$\cos\theta\sin i = 2\sqrt{1-\zeta^2-\psi^2}\left(\psi\cos\lambda + \zeta\sin\lambda\right) \tag{16}$$

With the trigonometric expressions established above, the inclination of the chief spacecraft may be written

$$i = 2\tan^{-1}\left(\sqrt{\frac{\zeta^2+\psi^2}{1-\zeta^2-\psi^2}}\right) \tag{17}$$

The first variation of the chief inclination i is therefore expressed as

$$\delta i = \frac{2}{\zeta^2+\psi^2}\left(\zeta\delta\zeta + \psi\delta\psi\right)\sqrt{\frac{\zeta^2+\psi^2}{1-\zeta^2-\psi^2}} \tag{18}$$

Recalling that the first variation of the expression $\cos i = 1 - 2\zeta^2 - 2\psi^2$ is equivalent to $\sin i\ \delta i = 4\zeta\delta\zeta + 4\psi\delta\psi$, trigonometric development of intermediate results is employed to transform the $\sin\theta\ \delta i$ term of Equation (6):

$$\sin\theta = \sin\lambda\cos\Omega - \cos\lambda\sin\Omega \tag{19a}$$
$$\sin(i/2)\sin\theta = \psi\sin\lambda - \zeta\cos\lambda \tag{19b}$$
$$2\cos(i/2)\sin(i/2)\sin\theta = 2\cos(i/2)\left(\psi\sin\lambda - \zeta\cos\lambda\right) \tag{19c}$$
$$\sin i\sin\theta = 2\cos(i/2)\left(\psi\sin\lambda - \zeta\cos\lambda\right) \tag{19d}$$

Multiplying each side of the above expression for $\sin i\sin\theta$ by the factor δi^2, the developed identity becomes

$$\left(4\zeta\delta\zeta + 4\psi\delta\psi\right)\sin\theta\ \delta i = 2\sqrt{1-\zeta^2-\psi^2}\left(\psi\sin\lambda - \zeta\cos\lambda\right)\delta i^2 \tag{20}$$

Substituting Equation (18) into the right-hand side of the above expression, the developed identity is finalized:

$$\sin\theta\,\delta i = -\frac{2}{\sqrt{1-\zeta^2-\psi^2}}\left[\frac{\zeta\cos\lambda-\psi\sin\lambda}{\zeta^2+\psi^2}\right](\zeta\delta\zeta+\psi\delta\psi) \tag{21}$$

Substituting Equations (49), (12), (16), and (21) into Equation (6), the cross-track component of position is

$$z = \frac{2r}{\sqrt{1-\zeta^2-\psi^2}}\Big\{\left[\left(\psi^2-1\right)\cos\lambda+\zeta\psi\sin\lambda\right]\delta\zeta-\left[\left(\zeta^2-1\right)\sin\lambda+\zeta\psi\cos\lambda\right]\delta\psi\Big\} \tag{22}$$

Derivation of the linear mapping from nonsingular orbit element differences to Hill frame position is complete.

II.B Mapping to Hill Frame Velocity

Relative Hill frame Cartesian velocity $(\dot{x},\dot{y},\dot{z})$ is expressed in terms of classical orbit element differences as:[16]

$$\dot{x} = \delta V_r \tag{23}$$

$$\dot{y} = \delta V_t - \dot{\theta}x + \left(\frac{V_r}{r}\right)y \tag{24}$$

$$\dot{z} = \left(V_t\cos\theta + V_r\sin\theta\right)\delta i + \left(V_t\sin\theta - V_r\cos\theta\right)\sin i\,\delta\Omega \tag{25}$$

Recalling Equation (9) for the radial velocity component of the chief craft, the first variation of V_r is expressed with nonsingular orbital element differences; simplification gives the Cartesian radial component of velocity:

$$\dot{x} = -\frac{V_r}{2a}\delta a + \left(V_r a\xi - h\cos\lambda\right)\frac{\delta\xi}{p} + \left(V_r a\eta + h\sin\lambda\right)\frac{\delta\eta}{p} + \left(\frac{1}{r}-\frac{1}{p}\right)h\delta\lambda \tag{26}$$

The form of Equation (26) is analogous to that of the radial velocity $\dot{x}$ mapping with classical orbital element differences.[10] In this development, the first variation of the specific angular momentum h of the chief craft is expressed by recalling that $h=\sqrt{\mu p}$, where μ denotes the gravitational parameter of the central body:

$$\delta h = \frac{h}{2p}\delta p \tag{27}$$

Recalling that the semi-latus rectum is cast as $p = a\left(1-\xi^2-\eta^2\right)$, the first variation of this parameter is

$$\delta p = \left(1-\xi^2-\eta^2\right)\delta a - 2a\xi\delta\xi - 2a\eta\delta\eta \tag{28}$$

Utilizing Equation (10) for the chief's transverse velocity component, the first variation of V_t is simplified to

$$\delta V_t = -\frac{V_t}{2a}\delta a + \left(V_t a\xi + h\sin\lambda\right)\frac{\delta\xi}{p} + \left(V_t a\eta + h\cos\lambda\right)\frac{\delta\eta}{p} - V_r\delta\lambda \tag{29}$$

Substituting Equations (11), (14), and (29) into Equation (24) and employing the specific angular momentum relationship $\dot{\theta}=h/r^2$, the Cartesian in-track component of velocity for the deputy object may be formulated:

$$\dot{y} = -\frac{3V_t}{2a}\delta a + \left(3V_t a\xi + 2h\sin\lambda\right)\frac{\delta\xi}{p} + \left(3V_t a\eta + 2h\cos\lambda\right)\frac{\delta\eta}{p} - 2V_r\psi\delta\zeta + 2V_r\zeta\delta\psi - V_r\delta\lambda \tag{30}$$

In a manner procedurally equivalent to that used in the development of Equation (21), it may be shown that

$$\cos\theta\,\delta i = -\frac{2}{\sqrt{1-\zeta^2-\psi^2}}\left[\frac{\zeta\sin\lambda+\psi\cos\lambda}{\zeta^2+\psi^2}\right](\zeta\delta\zeta+\psi\delta\psi) \tag{31}$$

Furthermore, recalling the trigonometric identities determined previously for the Cartesian position mapping:

$$\cos\theta\sin i = 2\cos(i/2)\left(\psi\cos\lambda+\zeta\sin\lambda\right) \tag{32}$$

$$\sin\theta\sin i = 2\cos(i/2)\left(\psi\sin\lambda-\zeta\cos\lambda\right) \tag{33}$$

Transformation of Equation (25) is thus performed by substituting in the intermediate expressions provided by Equations (12), (21), (31), (32), and (33). The cross-track component of velocity for the deputy is thereby

$$\begin{aligned}\dot{z} = &\frac{2h}{p\sqrt{1-\zeta^2-\psi^2}}\left[\left(1-\psi^2\right)\left(\xi+\sin\lambda\right)+\zeta\psi\left(\eta+\cos\lambda\right)\right]\delta\zeta \\ &+\frac{2h}{p\sqrt{1-\zeta^2-\psi^2}}\left[\left(1-\zeta^2\right)\left(\eta+\cos\lambda\right)+\zeta\psi\left(\xi+\sin\lambda\right)\right]\delta\psi\end{aligned} \tag{34}$$

Derivation of the linear mapping from nonsingular orbit element differences to Hill frame velocity is complete; note that this development could have been equivalently performed through the differentiation of the position mapping given by Equations (11), (14), and (22), with substitution of the first variation in the drift rate $\delta\dot{\lambda}$.

II.C Mapping to Hill Frame State

The development of the linear mapping from the nonsingular orbital element differences $\left(\delta a, \delta\xi, \delta\eta, \delta\zeta, \delta\psi, \delta\lambda\right)^T$ to the relative Cartesian state expressed within the rotating Hill frame of the chief spacecraft is now complete:

$$\begin{aligned}
x &= \frac{1}{\alpha}\delta a - \rho\left(2a\xi + r\sin\lambda\right)\delta\xi - \rho\left(2a\eta + r\cos\lambda\right)\delta\eta + r\nu\delta\lambda \\
y &= r\left(-2\psi\delta\zeta + 2\zeta\delta\psi + \delta\lambda\right) \\
z &= \frac{2r}{\sqrt{1-\zeta^2-\psi^2}}\left\{\left[\left(\psi^2-1\right)\cos\lambda + \zeta\psi\sin\lambda\right]\delta\zeta - \left[\left(\zeta^2-1\right)\sin\lambda + \zeta\psi\cos\lambda\right]\delta\psi\right\} \\
\dot{x} &= -\frac{V_r}{2a}\delta a + \left(V_r a\xi - h\cos\lambda\right)\frac{\delta\xi}{p} + \left(V_r a\eta + h\sin\lambda\right)\frac{\delta\eta}{p} + \left(\frac{1}{r}-\frac{1}{p}\right)h\delta\lambda \\
\dot{y} &= -\frac{3V_t}{2a}\delta a + \left(3V_t a\xi + 2h\sin\lambda\right)\frac{\delta\xi}{p} + \left(3V_t a\eta + 2h\cos\lambda\right)\frac{\delta\eta}{p} - 2V_r\psi\delta\zeta + 2V_r\zeta\delta\psi - V_r\delta\lambda \\
\dot{z} &= \frac{2h}{p\sqrt{1-\zeta^2-\psi^2}}\left[\left(1-\psi^2\right)\left(\xi+\sin\lambda\right)+\zeta\psi\left(\eta+\cos\lambda\right)\right]\delta\zeta \\
&\quad + \frac{2h}{p\sqrt{1-\zeta^2-\psi^2}}\left[\left(1-\zeta^2\right)\left(\eta+\cos\lambda\right)+\zeta\psi\left(\xi+\sin\lambda\right)\right]\delta\psi
\end{aligned} \tag{35}$$

The above transformation expressions satisfy the linear mapping provided in Equation (2) for the nonsingular set of orbital element differences given by Equation (3). The relative Hill frame state of the examined deputy object may thereby be expressed as a function of the chief orbital elements $\boldsymbol{e}_c$ and the instantaneous element differences $\delta\boldsymbol{e}$. Note this description accommodates perturbations and is valid for chief eccentricities $e_c \geq 0$.[10]

II.D Validation of Linear Mapping

Validation of the linear mapping from nonsingular orbital element differences to relative Hill frame Cartesian state is performed through quantitative comparison of the deputy positions and velocities computed with (*a*) the complete linear mapping provided within Equation (35), and (*b*) inertial differencing of the propagated chief and deputy states, with transformation of the resultant deputy states into the relative Hill frame of the chief. The simulation is conducted assuming a point-mass Earth without orbital perturbations and the initial conditions listed in Table 1, representative of nominal chief orbits in the geostationary regime. Propagated error in the Hill frame state of the deputy, as computed with the developed linear mapping from nonsingular orbit element differences, is depicted in Figure 2. The mapping is in strong agreement with the exact relative motion solution obtained with inertial differencing – the oscillatory errors in relative position are of $\mathcal{O}(10^{-3})$ m, while errors in Hill frame velocity are of $\mathcal{O}(10^{-6})$ m/s. This linear mapping therefore approximates the full nonlinear motion experienced by the deputy with a degree of accuracy appropriate for the verification of this formulation. Note that because temporal evolution of the error remains bounded, this mapping does not decay in time. As a basis for comparison, propagated error in the Hill frame Cartesian state of the deputy, as computed with the classical Hill/Clohessy-Wiltshire (HCW) equations of relative motion, is illustrated in Figure 3.

The HCW formulation assumes a circular chief ($e_c = 0$) and relative motion in the linear regime:[10]

$$\begin{aligned} \ddot{x} - 2n\dot{y} - 3n^2 x &= 0 \\ \ddot{y} + 2n\dot{x} &= 0 \\ \ddot{z} + n^2 z &= 0 \end{aligned} \tag{36}$$

where $n = \sqrt{\mu/r^3}$ is the mean motion of the chief. Propagated errors in Hill frame position are of two orders of magnitude higher than the deviations achieved with the linear mapping; secular growth experienced in the in-track error component is a consequence of the weak ellipticity of the chief orbit utilized for this simulation. The HCW description of relative motion thus temporally decays even with weakly-eccentric chief orbits; the linear mapping developed within this analysis does not impose this restriction upon the chief, thereby offering a more accurate and adaptable description of relative motion well-suited for chief orbits in the GEO regime.

Table 1: Initial conditions for validating linear mapping.

Element	**Chief** ($\boldsymbol{e}_c$)	**Deputy** ($\boldsymbol{e}_d$)	$\delta\boldsymbol{e}$
a	42164 km	42164 km	0 km
e	0.0001	0.00011	0.00001
i	0.001°	0.002°	0.001°
Ω	0°	0°	0°
ω	0°	0°	0°
f_0	0°	0°	0°

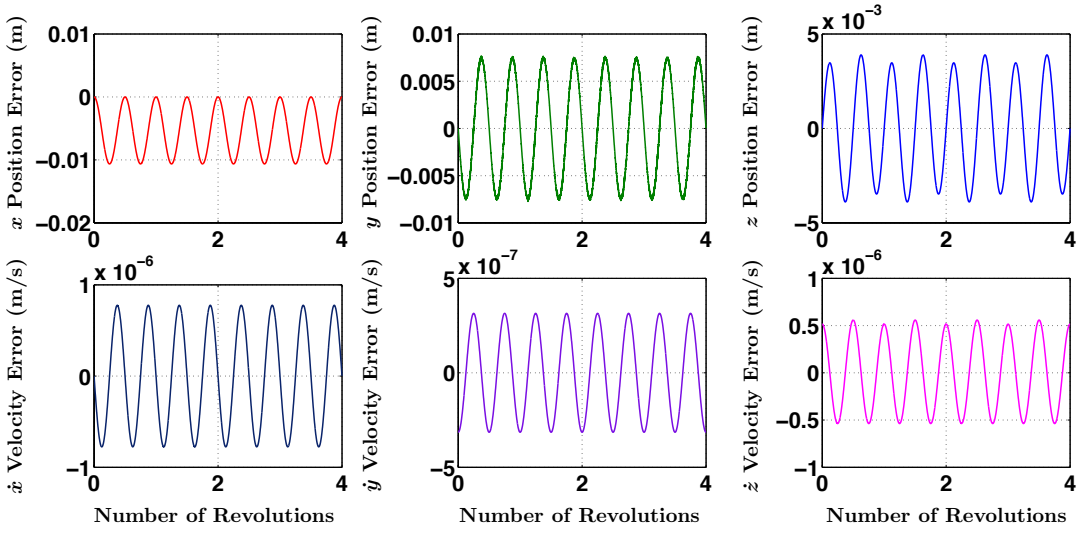

Figure 2: Temporal error in relative Hill frame state of deputy as computed with linear mapping.

III Development of Gaussian Variational Equations

The Gaussian variational equations for nonconservative perturbations to the nonsingular orbital elements are developed to characterize the sensitivities of the elements to thrusting events – this formulation quantifies rates of change

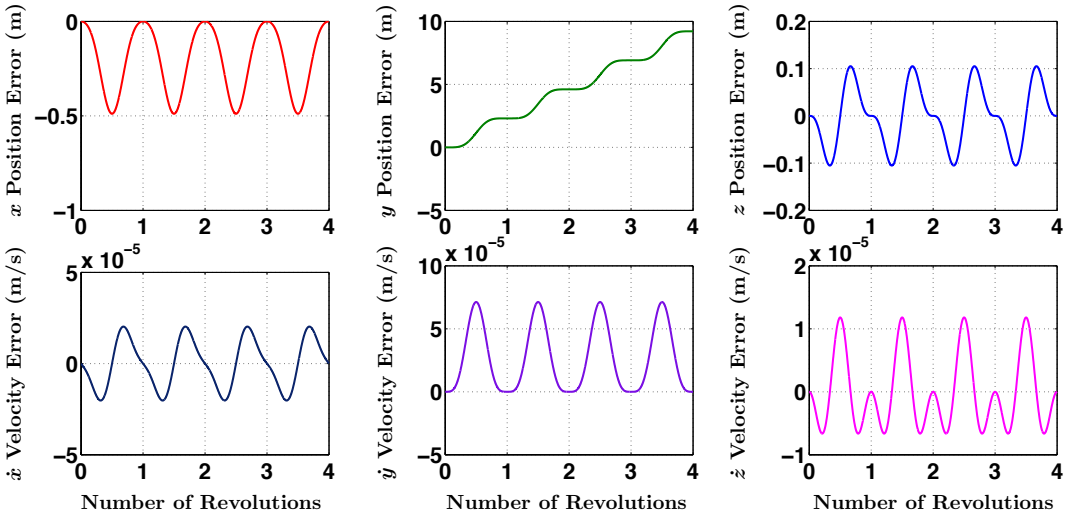

Figure 3: Temporal error in relative Hill frame state of deputy as computed with HCW equations.

of the elements in the presence of nonconservative accelerations. Differentiating Equations (1):

$$\frac{\mathrm{d}\xi}{\mathrm{d}t} = \sin(\omega+\Omega)\frac{\mathrm{d}e}{\mathrm{d}t} + \eta\left(\frac{\mathrm{d}\omega}{\mathrm{d}t} + \frac{\mathrm{d}\Omega}{\mathrm{d}t}\right) \tag{37}$$

$$\frac{\mathrm{d}\eta}{\mathrm{d}t} = \cos(\omega+\Omega)\frac{\mathrm{d}e}{\mathrm{d}t} - \xi\left(\frac{\mathrm{d}\omega}{\mathrm{d}t} + \frac{\mathrm{d}\Omega}{\mathrm{d}t}\right) \tag{38}$$

$$\frac{\mathrm{d}\zeta}{\mathrm{d}t} = \frac{1}{2}\cos(i/2)\sin(\Omega)\frac{\mathrm{d}i}{\mathrm{d}t} + \psi\frac{\mathrm{d}\Omega}{\mathrm{d}t} \tag{39}$$

$$\frac{\mathrm{d}\psi}{\mathrm{d}t} = \frac{1}{2}\cos(i/2)\cos(\Omega)\frac{\mathrm{d}i}{\mathrm{d}t} - \zeta\frac{\mathrm{d}\Omega}{\mathrm{d}t} \tag{40}$$

$$\frac{\mathrm{d}\lambda}{\mathrm{d}t} = \frac{\mathrm{d}f}{\mathrm{d}t} + \frac{\mathrm{d}\omega}{\mathrm{d}t} + \frac{\mathrm{d}\Omega}{\mathrm{d}t} \tag{41}$$

Recalling the well-known Gaussian variational equations for the classical Keplerian element set $(a, e, i, \Omega, \omega, f)$:[10]

$$\frac{\mathrm{d}a}{\mathrm{d}t} = \frac{2a^2}{h}\left(e\sin f a_r + \frac{p}{r}a_i\right) \tag{42}$$

$$\frac{\mathrm{d}e}{\mathrm{d}t} = \frac{1}{h}\left(p\sin f a_r + \left[(p+r)\cos f + re\right]a_i\right) \tag{43}$$

$$\frac{\mathrm{d}i}{\mathrm{d}t} = \frac{r\cos\theta}{h}a_c \tag{44}$$

$$\frac{\mathrm{d}\Omega}{\mathrm{d}t} = \frac{r\sin\theta}{h\sin i}a_c \tag{45}$$

$$\frac{\mathrm{d}\omega}{\mathrm{d}t} = \frac{1}{he}\left[-p\cos f a_r + (p+r)\sin f a_i\right] - \frac{r\sin\theta\cos i}{h\sin i}a_c \tag{46}$$

$$\frac{\mathrm{d}f}{\mathrm{d}t} = \frac{h}{r^2} + \frac{1}{he}\left[p\cos f a_r - (p+r)\sin f a_i\right] \tag{47}$$

wherein $\boldsymbol{a}_d \equiv a_r\hat{\boldsymbol{o}}_r + a_i\hat{\boldsymbol{o}}_i + a_c\hat{\boldsymbol{o}}_c$ denotes the nonconservative disturbing acceleration expressed in the local orbit radial ($\hat{\boldsymbol{o}}_r$), in-track ($\hat{\boldsymbol{o}}_i$), and cross-track ($\hat{\boldsymbol{o}}_c$) frame of reference. As the semi-major axis a is used in the nonsingular element set, transformation of Equation (42) provides the first variational equation. Recalling the formulation $e\sin f = \eta\sin\lambda - \xi\cos\lambda$, the rate of change of the perturbed semi-major axis is rewritten as

$$\frac{\mathrm{d}a}{\mathrm{d}t} = \frac{2a^2}{h}\left[\left(\eta\sin\lambda - \xi\cos\lambda\right)a_r + \frac{p}{r}a_i\right] \tag{48}$$

wherein h and p denote specific angular momentum and semi-latus rectum, respectively, and the radius r is

$$r = \frac{a\left(1-\xi^2-\eta^2\right)}{1+\eta\cos\lambda+\xi\sin\lambda} \tag{49}$$

Substituting Equations (43), (45), and (46) into Equation (37), the rate of change of the parameter ξ is cast:

$$\frac{\mathrm{d}\xi}{\mathrm{d}t} = \frac{1}{h}\left(-p\cos\lambda\, a_r + \big[(p+r)\sin\lambda + r\xi\big]a_i - r\eta\left[\frac{\zeta\cos\lambda-\psi\sin\lambda}{\sqrt{1-\zeta^2-\psi^2}}\right]a_c\right) \tag{50}$$

where the identities $\sin(i/2)\sin\theta = \psi\sin\lambda - \zeta\cos\lambda$ and $\cos(i/2) = \sqrt{1-\zeta^2-\psi^2}$ have been employed in the nontrivial simplification. Similarly, it may be shown that the rate of change of the parameter η is written as

$$\frac{\mathrm{d}\eta}{\mathrm{d}t} = \frac{1}{h}\left(p\sin\lambda\, a_r + \big[(p+r)\cos\lambda + r\eta\big]a_i + r\xi\left[\frac{\zeta\cos\lambda-\psi\sin\lambda}{\sqrt{1-\zeta^2-\psi^2}}\right]a_c\right) \tag{51}$$

The parameters ξ and η contain the eccentricity and the Euler angles ω and Ω, and thus may be perturbed by radial, in-track, and cross-track accelerations simultaneously. Substituting Equations (44) and (45) into Equation (39), the rate of change of the parameter ζ is expressed as

$$\frac{\mathrm{d}\zeta}{\mathrm{d}t} = \frac{r}{2h\cos(i/2)}\left[\sin\theta\cos\Omega + \cos^2(i/2)\cos\theta\sin\Omega\right]a_c \tag{52}$$

Implementing $\cos^2(i/2) = 1-\sin^2(i/2)$ and the expression $\sin(i/2)\cos\theta = \psi\cos\lambda + \zeta\sin\lambda$, and recalling from trigonometry that $\sin\theta\cos\Omega + \cos\theta\sin\Omega = \sin(\theta+\Omega) = \sin(f+\omega+\Omega) = \sin\lambda$, this rate may be recast:

$$\frac{\mathrm{d}\zeta}{\mathrm{d}t} = \frac{r}{2h\sqrt{1-\zeta^2-\psi^2}}\Big[(1-\zeta^2)\sin\lambda - \zeta\psi\cos\lambda\Big]a_c \tag{53}$$

In an equivalent manner, the rate of change of the analogous parameter ψ may be converted into the following:

$$\frac{\mathrm{d}\psi}{\mathrm{d}t} = \frac{r}{2h\sqrt{1-\zeta^2-\psi^2}}\Big[(1-\psi^2)\cos\lambda - \zeta\psi\sin\lambda\Big]a_c \tag{54}$$

The parameters ζ and ψ contain the Euler angles i and Ω, and are only influenced by cross-track accelerations. Lastly, the rate of change of the longitude parameter λ in Equation (41) is transformed into the following:

$$\frac{\mathrm{d}\lambda}{\mathrm{d}t} = \frac{h}{r^2} - \frac{r}{h}\left[\frac{\zeta\cos\lambda-\psi\sin\lambda}{\sqrt{1-\zeta^2-\psi^2}}\right]a_c \tag{55}$$

Note that perturbed variation in the longitude parameter λ may only be induced with cross-track acceleration. Development of the Gaussian variational equations for the nonsingular element set $(a,\xi,\eta,\zeta,\psi,\lambda)$ is complete; this formulation quantifies sensitivities of the elements to nonconservative disturbances and is summarized:

$$\frac{\mathrm{d}a}{\mathrm{d}t} = \frac{2a^2}{h}\left[(\eta\sin\lambda - \xi\cos\lambda)\,a_r + \frac{p}{r}a_i\right] \tag{56}$$

$$\frac{\mathrm{d}\xi}{\mathrm{d}t} = \frac{1}{h}\left(-p\cos\lambda\, a_r + \big[(p+r)\sin\lambda + r\xi\big]a_i - r\eta\left[\frac{\zeta\cos\lambda-\psi\sin\lambda}{\sqrt{1-\zeta^2-\psi^2}}\right]a_c\right) \tag{57}$$

$$\frac{\mathrm{d}\eta}{\mathrm{d}t} = \frac{1}{h}\left(p\sin\lambda\, a_r + \big[(p+r)\cos\lambda + r\eta\big]a_i + r\xi\left[\frac{\zeta\cos\lambda-\psi\sin\lambda}{\sqrt{1-\zeta^2-\psi^2}}\right]a_c\right) \tag{58}$$

$$\frac{\mathrm{d}\zeta}{\mathrm{d}t} = \frac{r}{2h\sqrt{1-\zeta^2-\psi^2}}\Big[(1-\zeta^2)\sin\lambda - \zeta\psi\cos\lambda\Big]a_c \tag{59}$$

$$\frac{\mathrm{d}\psi}{\mathrm{d}t} = \frac{r}{2h\sqrt{1-\zeta^2-\psi^2}}\Big[(1-\psi^2)\cos\lambda - \zeta\psi\sin\lambda\Big]a_c \tag{60}$$

$$\frac{\mathrm{d}\lambda}{\mathrm{d}t} = \frac{h}{r^2} - \frac{r}{h}\left[\frac{\zeta\cos\lambda-\psi\sin\lambda}{\sqrt{1-\zeta^2-\psi^2}}\right]a_c \tag{61}$$

The Gaussian variational equations for the element set presented in Equations (1) are nonsingular for circular orbits with zero inclination, and are thus well-suited to describing perturbed motion within the GEO regime. This formulation furthermore eliminates the numerical difficulties associated with the variational equations in classical Keplerian elements for weakly-eccentric orbits, and therefore should be employed in those situations. These variational equations are convenient for quantifying effects of a control thrust on each of the nonsingular elements, and are thereby implemented as the basis for development of the impulsive feedback control scheme.

IV Development of Impulsive Feedback Control Law

An N-impulse feedback control law is now developed to present methodology for controlling relative orbit tracking errors at discrete positions in orbit with pre-determined impulsive maneuvers, rather than providing a continuous thrusting control effort. Modifying the Gaussian variational equations for the nonsingular orbit elements with an impulsive $\Delta \boldsymbol{v}$ thrust in the Hill frame, and considering only the perturbed response of the longitude parameter rate $\dot{\lambda}$:

$$\Delta a = \frac{2a^2}{h}\left[(\eta \sin\lambda - \xi\cos\lambda)\,\Delta v_r + \frac{p}{r}\Delta v_i\right] \tag{62}$$

$$\Delta \xi = \frac{1}{h}\left(-p\cos\lambda\,\Delta v_r + \left[(p+r)\sin\lambda + r\xi\right]\Delta v_i - r\eta\left[\frac{\zeta\cos\lambda - \psi\sin\lambda}{\sqrt{1-\zeta^2-\psi^2}}\right]\Delta v_c\right) \tag{63}$$

$$\Delta \eta = \frac{1}{h}\left(p\sin\lambda\,\Delta v_r + \left[(p+r)\cos\lambda + r\eta\right]\Delta v_i + r\xi\left[\frac{\zeta\cos\lambda - \psi\sin\lambda}{\sqrt{1-\zeta^2-\psi^2}}\right]\Delta v_c\right) \tag{64}$$

$$\Delta \zeta = \frac{r}{2h\sqrt{1-\zeta^2-\psi^2}}\Big[(1-\zeta^2)\sin\lambda - \zeta\psi\cos\lambda\Big]\Delta v_c \tag{65}$$

$$\Delta \psi = \frac{r}{2h\sqrt{1-\zeta^2-\psi^2}}\Big[(1-\psi^2)\cos\lambda - \zeta\psi\sin\lambda\Big]\Delta v_c \tag{66}$$

$$\Delta \lambda = -\frac{r}{h}\left[\frac{\zeta\cos\lambda - \psi\sin\lambda}{\sqrt{1-\zeta^2-\psi^2}}\right]\Delta v_c \tag{67}$$

Note that Equations (65)-(66) can be rewritten in the form

$$\Delta \zeta = \frac{r\sin\lambda}{2h}\sqrt{1-\zeta^2-\psi^2}\Delta v_c + \frac{\psi}{2}\Delta\lambda \tag{68}$$

$$\Delta \psi = \frac{r\cos\lambda}{2h}\sqrt{1-\zeta^2-\psi^2}\Delta v_c - \frac{\zeta}{2}\Delta\lambda \tag{69}$$

Corrections in the longitude parameter λ are linearly-related to corrections in the ζ and ψ parameters; thus, errors in the longitude parameter, and consequently the true anomaly f, cannot be independently controlled with an impulsive feedback scheme constructed around this set of nonsingular elements. Note, however, that the true anomaly can be corrected by performing a phasing maneuver in which the semi-major axis is raised or lowered temporarily, to provide relative drift for the required phase shift. Thus, corrections in semi-major axis may be used for correcting the true anomaly; the N-impulse feedback law accommodates this correction.

An N-impulse approach is implemented for this study to alleviate difficulties arising from the complexity of the nonsingular variational equations given in Equations (56)-(61). Reference 1 creates an impulsive firing scheme in which subsets of the full Keplerian element set are corrected simultaneously, by studying Gauss's variational equations to determine ideal times at which to execute the corrective burns. However, with these nonsingular elements, innate complexity of the variational equations renders an analogous analytical solution difficult to determine. Thus, rather than seeking an analytical solution for relative orbit corrections, a swift numerical method that will determine the ideal burn locations for achieving the desired corrections is sought.

IV.A Formulation of Control Strategy

In a manner analogous to that utilized in Reference 1, nonsingular element errors $\Delta \boldsymbol{e} \equiv (\Delta a, \Delta\xi, \Delta\eta, \Delta\zeta, \Delta\psi)^T$ are held fixed at the beginning of the time frame of correction. An N-impulse sequence is then implemented over the current revolution, where the burns are executed at uniform increments in true anomaly, such that $N = 360^\circ / f_{\Delta v}$,

where $f_{\Delta v}$ is the specified true anomaly increment expressed in degrees per burn.[b] Therefore, for the j^{th} impulse $\Delta \boldsymbol{v}_j \equiv (\Delta v_r^j, \Delta v_i^j, \Delta v_c^j)^T$, the contribution to the nonsingular element corrections become

$$\Delta a_j = \frac{2a^2}{h}\left[\left(\eta \sin\lambda_j - \xi\cos\lambda_j\right)\Delta v_r^j + \frac{p}{r_j}\Delta v_i^j\right] \tag{70}$$

$$\Delta \xi_j = \frac{1}{h}\left(-p\cos\lambda_j\,\Delta v_r^j + \left[(p+r_j)\sin\lambda_j + r_j\xi\right]\Delta v_i^j - r_j\eta\left[\frac{\zeta\cos\lambda_j - \psi\sin\lambda_j}{\sqrt{1-\zeta^2-\psi^2}}\right]\Delta v_c^j\right) \tag{71}$$

$$\Delta \eta_j = \frac{1}{h}\left(p\sin\lambda_j\,\Delta v_r^j + \left[(p+r_j)\cos\lambda_j + r_j\eta\right]\Delta v_i^j + r_j\xi\left[\frac{\zeta\cos\lambda_j - \psi\sin\lambda_j}{\sqrt{1-\zeta^2-\psi^2}}\right]\Delta v_c^j\right) \tag{72}$$

$$\Delta \zeta_j = \frac{r_j}{2h\sqrt{1-\zeta^2-\psi^2}}\Big[(1-\zeta^2)\sin\lambda_j - \zeta\psi\cos\lambda_j\Big]\Delta v_c^j \tag{73}$$

$$\Delta \psi_j = \frac{r_j}{2h\sqrt{1-\zeta^2-\psi^2}}\Big[(1-\psi^2)\cos\lambda_j - \zeta\psi\sin\lambda_j\Big]\Delta v_c^j \tag{74}$$

where the subscript j denotes conditions at the execution of the j^{th} burn; parameters without this subscript, including the nonsingular elements of the maneuvering spacecraft, are fixed at the beginning of the maneuver sequence in Equations (70)-(74). As this piecewise-constant assumption neglects the influence of each impulse on the nonsingular elements, this control strategy is designed to significantly reduce, not completely eliminate, errors in the nonsingular elements over a single revolution. Multiple correction orbits may be readily employed to fully nullify the errors $\Delta \boldsymbol{e}$ if desired, by fixing the residual errors at the beginning of each correction orbit, and implementing an updated N-impulse maneuver sequence for the current revolution, computed as follows.

For compactness, corrections to the elements due to the j^{th} burn in Equations (70)-(74) are rewritten as

$$\Delta a_j = \Delta a_j^r \Delta v_r^j + \Delta a_j^i \Delta v_i^j \tag{75}$$

$$\Delta \xi_j = \Delta \xi_j^r \Delta v_r^j + \Delta \xi_j^i \Delta v_i^j + \Delta \xi_j^c \Delta v_c^j \tag{76}$$

$$\Delta \eta_j = \Delta \eta_j^r \Delta v_r^j + \Delta \eta_j^i \Delta v_i^j + \Delta \eta_j^c \Delta v_c^j \tag{77}$$

$$\Delta \zeta_j = \Delta \zeta_j^c \Delta v_c^j \tag{78}$$

$$\Delta \psi_j = \Delta \psi_j^c \Delta v_c^j \tag{79}$$

[b] In this sense, the N-impulse sequence may be treated as a discretization of a general continuous, low-thrust control effort.

where the following definitions have been used:

$$\Delta a_j^r \equiv \frac{2a^2}{h}\left(\eta \sin\lambda_j - \xi \cos\lambda_j\right) \tag{80}$$

$$\Delta a_j^i \equiv \frac{2a^2 p}{h r_j} \tag{81}$$

$$\Delta \xi_j^r \equiv -\frac{p}{h}\cos\lambda_j \tag{82}$$

$$\Delta \xi_j^i \equiv \frac{1}{h}\left[(p + r_j)\sin\lambda_j + r_j \xi\right] \tag{83}$$

$$\Delta \xi_j^c \equiv -\frac{r_j \eta}{h}\left[\frac{\zeta\cos\lambda_j - \psi\sin\lambda_j}{\sqrt{1-\zeta^2-\psi^2}}\right] \tag{84}$$

$$\Delta \eta_j^r \equiv \frac{p}{h}\sin\lambda_j \tag{85}$$

$$\Delta \eta_j^i \equiv \frac{1}{h}\left[(p + r_j)\cos\lambda_j + r_j \eta\right] \tag{86}$$

$$\Delta \eta_j^c \equiv \frac{r_j \xi}{h}\left[\frac{\zeta\cos\lambda_j - \psi\sin\lambda_j}{\sqrt{1-\zeta^2-\psi^2}}\right] \tag{87}$$

$$\Delta \zeta_j^c \equiv \frac{r_j}{2h\sqrt{1-\zeta^2-\psi^2}}\Big[(1-\zeta^2)\sin\lambda_j - \zeta\psi\cos\lambda_j\Big] \tag{88}$$

$$\Delta \psi_j^c \equiv \frac{r_j}{2h\sqrt{1-\zeta^2-\psi^2}}\Big[(1-\psi^2)\cos\lambda_j - \zeta\psi\sin\lambda_j\Big] \tag{89}$$

The total element corrections $\Delta \boldsymbol{e} = \sum_{j=1}^{N} \Delta \boldsymbol{e}_j$ due to the N impulses executed in the correction orbit become

$$\begin{pmatrix} \Delta a \\ \Delta \xi \\ \Delta \eta \\ \Delta \zeta \\ \Delta \psi \end{pmatrix} = \begin{pmatrix} \Delta a_1^r & \Delta a_1^i & 0 & \dots & \Delta a_j^r & \Delta a_j^i & 0 & \dots & \Delta a_N^r & \Delta a_N^i & 0 \\ \Delta \xi_1^r & \Delta \xi_1^i & \Delta \xi_1^c & \dots & \Delta \xi_j^r & \Delta \xi_j^i & \Delta \xi_j^c & \dots & \Delta \xi_N^r & \Delta \xi_N^i & \Delta \xi_N^c \\ \Delta \eta_1^r & \Delta \eta_1^i & \Delta \eta_1^c & \dots & \Delta \eta_j^r & \Delta \eta_j^i & \Delta \eta_j^c & \dots & \Delta \eta_N^r & \Delta \eta_N^i & \Delta \eta_N^c \\ 0 & 0 & \Delta \zeta_1^c & \dots & 0 & 0 & \Delta \zeta_j^c & \dots & 0 & 0 & \Delta \zeta_N^c \\ 0 & 0 & \Delta \psi_1^c & \dots & 0 & 0 & \Delta \psi_j^c & \dots & 0 & 0 & \Delta \psi_N^c \end{pmatrix} \begin{pmatrix} \Delta v_r^1 \\ \Delta v_i^1 \\ \Delta v_c^1 \\ \vdots \\ \Delta v_r^j \\ \Delta v_i^j \\ \Delta v_c^j \\ \vdots \\ \Delta v_r^N \\ \Delta v_i^N \\ \Delta v_c^N \end{pmatrix} \tag{90}$$

which may be written more compactly in the following form:

$$\Delta \boldsymbol{e} = [B(\boldsymbol{e}_j)]\Delta \boldsymbol{v}_{\text{seq}} \tag{91}$$

The objective of this feedback control strategy is to extract the N-impulse burn sequence $\Delta \boldsymbol{v}_{\text{seq}}$ that satisfies Equation (91) and simultaneously minimizes the fuel cost required to perform the corrective sequence. Note that $[B(\boldsymbol{e}_j)]$ is of dimension $5 \times 3N$ and cannot be inverted. To obtain the fuel-optimal N-impulse sequence, the following nonlinear programming (NLP) problem governing this feedback control strategy must be solved:

$$\begin{aligned} \underset{\Delta \boldsymbol{v}_{\text{seq}}}{\text{minimize}} \quad & J \equiv \sum_{j=1}^{N} ||\Delta \boldsymbol{v}_j|| = \sum_{j=1}^{N} \sqrt{\Delta v_r^j \Delta v_r^j + \Delta v_i^j \Delta v_i^j + \Delta v_c^j \Delta v_c^j} \\ \text{subject to} \quad & \boldsymbol{G} \equiv [B(\boldsymbol{e}_j)]\Delta \boldsymbol{v}_{\text{seq}} - \Delta \boldsymbol{e} = \boldsymbol{0} \end{aligned} \tag{92}$$

The solution to Equation (92) provides the minimum-fuel N-impulse sequence that mitigates the fixed errors $\Delta \boldsymbol{e}$ specified in the nonsingular elements. The gradient $\partial J / \partial \Delta \boldsymbol{v}_{\text{seq}}$ of the objective function thus follows as

$$\frac{\partial J}{\partial \Delta \boldsymbol{v}_{\text{seq}}} = \left(\begin{array}{ccccc} \dfrac{\Delta \boldsymbol{v}_1^T}{||\Delta \boldsymbol{v}_1||} & \cdots & \dfrac{\Delta \boldsymbol{v}_j^T}{||\Delta \boldsymbol{v}_j||} & \cdots & \dfrac{\Delta \boldsymbol{v}_N^T}{||\Delta \boldsymbol{v}_N||} \end{array} \right)^T \tag{93}$$

and the Jacobian $\partial \boldsymbol{G} / \partial \Delta \boldsymbol{v}_{\text{seq}}$ of the equality constraints within Equation (91) follows from Equation (92) as

$$\frac{\partial \boldsymbol{G}}{\partial \Delta \boldsymbol{v}_{\text{seq}}} = [B(\boldsymbol{e}_j)] \tag{94}$$

For this study, MATLAB's constrained minimization solver `fmincon` is utilized with the active set algorithm[c] to obtain a solution to the NLP problem provided in Equation (92). At the beginning of the correction orbit, the nonsingular element errors $\Delta \boldsymbol{e}$ are fixed, and $[B(\boldsymbol{e}_j)]$ is precomputed with the given longitude increments:

$$\lambda_j = f_0 + j f_{\Delta v} + \omega + \Omega, \quad j = 1, 2, \ldots, N \tag{95}$$

where f_0 is the true anomaly at the beginning of the maneuver sequence. The fuel-optimal maneuver sequence $\Delta \boldsymbol{v}_{\text{seq}}$ is then achieved by solving Equation (92) with `fmincon`, and is executed during the current revolution to mitigate the nonsingular element errors $\Delta \boldsymbol{e}$. For the test cases considered in this research, an initial guess of $\Delta \boldsymbol{v}_{\text{seq}} \equiv (\Delta \boldsymbol{v}_1, \ldots, \Delta \boldsymbol{v}_j, \ldots, \Delta \boldsymbol{v}_N)^T$ where $\Delta \boldsymbol{v}_j = (1, 1, 1)^T$ m/s $\forall\ j = 1, 2, \ldots, N$ is used for initializing the `fmincon` optimizer. As this initial guess is not guaranteed to be suitable for general scenarios, continuing efforts are focused on determining appropriate initial guesses for the maneuver sequence, to ensure optimizer convergence to a near-global minimum for the specified N-impulse control strategy.[d]

IV.B Examples of Control Strategy

Three test cases are presented to demonstrate the validity of the N-impulse control strategy developed above in Section IV.A. For simplicity, the deputy and chief are assumed to begin at the same location on equivalent orbits – therefore, the following examples simulate a deployment sequence in which the deputy is maneuvered to a different orbit relative to the chief. Since nonsingular elements are less intuitive to visualize, classic orbit element differences are specified for the test examples; the classical differences are converted into nonsingular differences required by this N-impulse control strategy. Thus, the nonsingular element set is used here as an "under-the-hood" mechanism for avoiding singularities in the variational equations for the classical elements. Note that the inertial J2000 frame is used for this control implementation – the optimal maneuver sequence must therefore be rotated from the local orbit frame to the inertial frame for integration and burn execution.

IV.B.1 Example 1: Inclination Change

The first example examines the case of an inclination change, in which it is known from basic orbit mechanics that the most efficient location for a plane change is at the equator crossing.[10] The initial deputy and desired conditions simulated for this example are provided in Table 2. Impulses are specified to occur every $f_{\Delta v} = 10^\circ$ for one revolution, such that $N = 36$ for this example. The optimal maneuver sequence is shown in Figure 4, and the corresponding error history of the classical orbit elements during execution of this sequence is shown in Figure 5. As anticipated, the radial and in-track burns remain small, while the cross-track burn spikes at the positions of the descending and ascending nodes, to raise the orbital plane and nullify all element errors. The total fuel cost for the sequence is $\Delta v_{\text{cost}} = 5.376$ cm/s, slightly larger than the single-impulse solution[17]

$$\Delta v_{\text{1-burn}} = 2 v_n \sin \frac{\Delta i}{2} \approx 5.367 \text{ cm/s} \tag{96}$$

where v_n is the spacecraft velocity magnitude at the node and $\Delta i = 0.001^\circ$ is the specified inclination change. Therefore, the control strategy approximately replicates the optimal single-impulse solution for this example.

[c] See `fmincon` documentation for explanation: `http://www.mathworks.com/help/toolbox/optim/ug/fmincon.html`

[d] Note that the optimizer *does not* vary N or the impulse locations in this formulation – only the burn magnitudes are varied.

Table 2: Initial and desired conditions for Example 1.

Element	Deputy	Desired	Δe_{coe}
a	42164 km	42164 km	0 km
e	0.0001	0.0001	0
i	10°	10.001°	0.001°
Ω	0°	0°	0°
ω	0°	0°	0°
f_0	0°	N/A	N/A

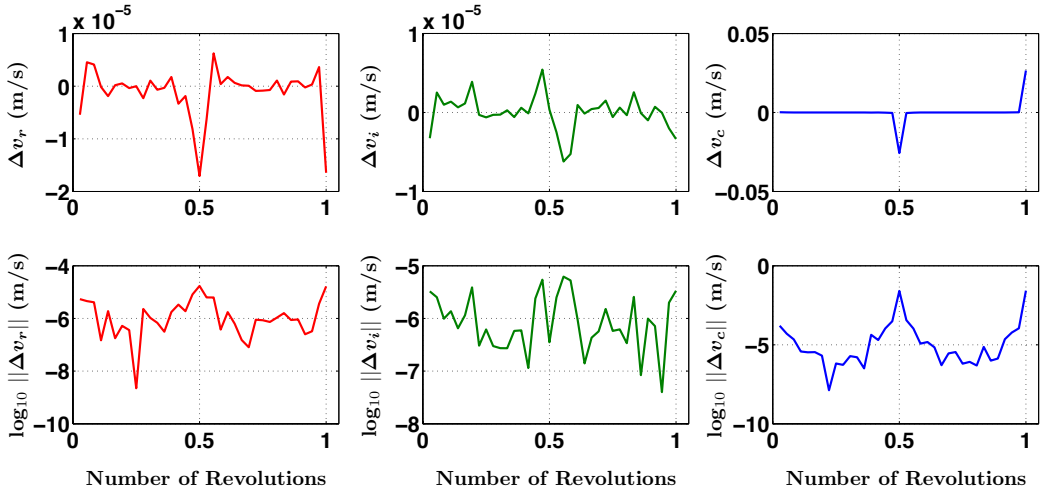

Figure 4: Fuel-optimal burn sequence determined by feedback control strategy for Example 1.

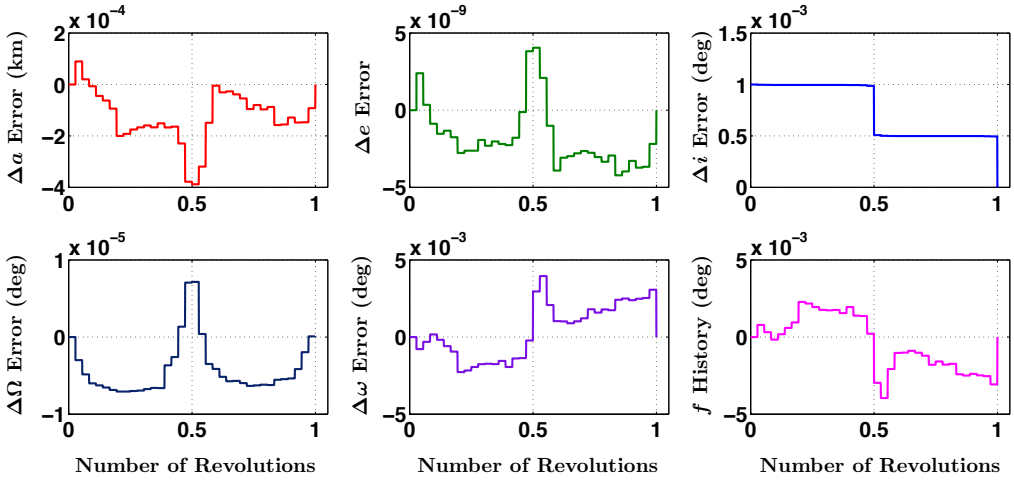

Figure 5: Error history of classical orbit elements during burn sequence execution for Example 1.

IV.B.2 Example 2: Circularizing at GEO

The second example examines the case of orbit raising and circularizing at the GEO altitude; such a transfer is useful when inserting into a near-geosynchronous orbit from an elliptic geostationary transfer orbit (GTO). The initial deputy and desired conditions simulated for this example are provided within Table 3. Impulses are specified to occur every $f_{\Delta v} = 30°$ for three revolutions, such that $N = 12$ burns per correction orbit for this example. The optimal maneuver sequence is shown in Figure 6, and the corresponding error history of the classical orbit elements during execution of this sequence is illustrated in Figure 7. For this solution, the in-track impulse magnitudes sharply increase at the descending and ascending nodes of the first revolution to circularize the orbit, and the radial burn magnitudes

sharply increase at the extreme latitudes of the second revolution to raise the orbit by nullifying errors in the semi-major axis. After execution of this optimal burn sequence, errors in the Euler angles Ω, i, ω are zeroed. The fuel cost for this solution is $\Delta v_{\text{cost}} = 15.70$ m/s.

Table 3: Initial and desired conditions for Example 2.

Element	Deputy	Desired	Δe_{coe}
a	42164 km	42164.1 km	0.1 km
e	0.01	0	-0.01
i	0.001°	0.001°	0°
Ω	0°	0°	0°
ω	0°	0°	0°
f_0	0°	N/A	N/A

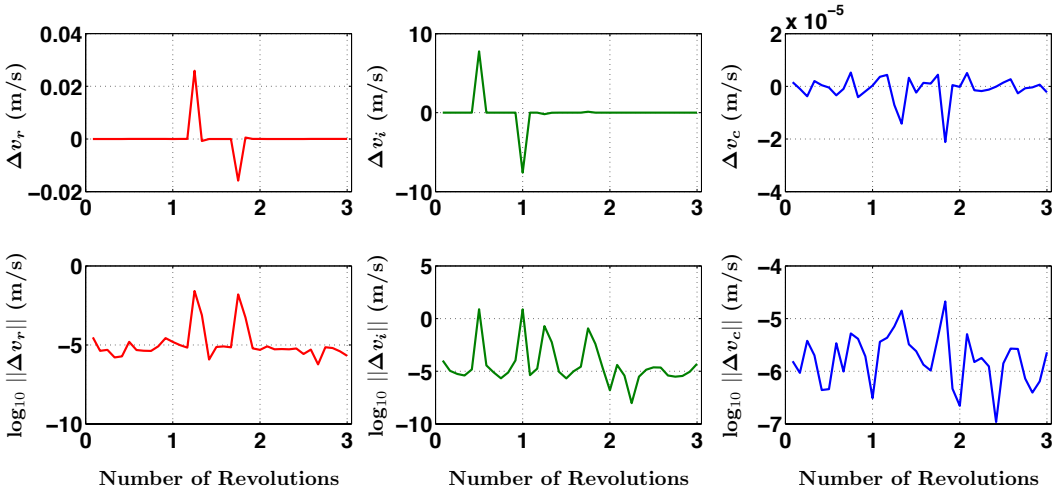

Figure 6: Fuel-optimal burn sequence determined by feedback control strategy for Example 2.

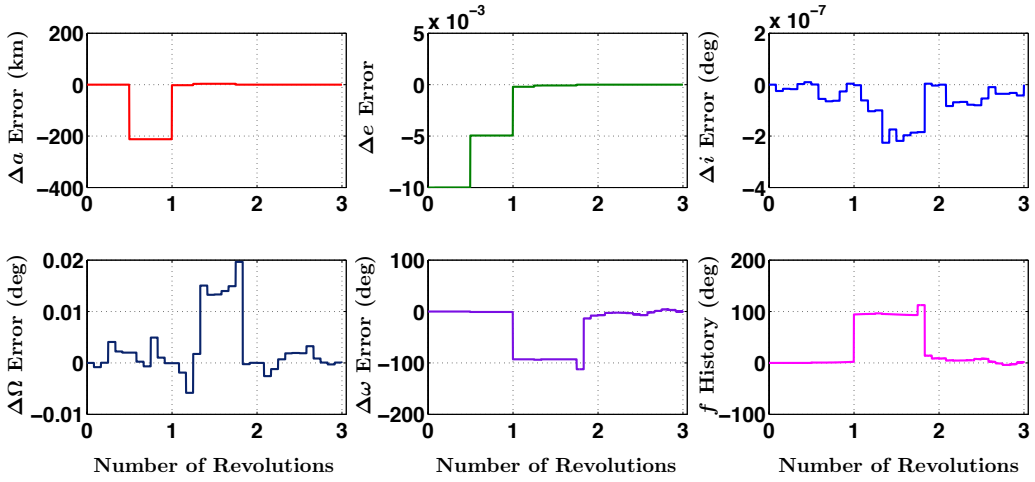

Figure 7: Error history of classical orbit elements during burn sequence execution for Example 2.

IV.B.3 Example 3: General Orbit Transfer

The third example examines the case of a general orbit transfer in which errors in the elements $(a, e, i, \Omega, \omega)$ are present and require correction with a multi-revolution maneuver sequence. The initial deputy and desired conditions

simulated for this example are provided in Table 4. Impulses are specified to occur every $f_{\Delta v} = 5^\circ$ for three revolutions, such that $N = 72$ per correction orbit for this example. The optimal maneuver sequence is shown in Figure 8, and the corresponding error history of the classical orbit elements during execution of this sequence is illustrated in Figure 9. For this maneuver solution, burn magnitudes in all three orbit frame directions sharply increase at the ascending and descending nodes during the first revolution, nullifying the errors in eccentricity and inclination. The semi-major axis is corrected after the second revolution, and the Euler angles Ω and ω are corrected after the complete three-revolution sequence. Note that the true anomaly deviates sizably by $\pm 2^\circ$ during execution – a phasing maneuver should thus be performed after this sequence to correct the true anomaly as desired. The total fuel cost for this maneuver sequence is $\Delta v_{\text{cost}} = 17.63$ m/s.

Table 4: Initial and desired conditions for Example 3.

Element	Deputy	Desired	Δe_{coe}
a	42164 km	42164.1 km	0.1 km
e	0.2	0.21	0.01
i	10°	10.1°	0.1°
Ω	0°	0.1°	0.1°
ω	0°	0.1°	0.1°
f_0	0°	N/A	N/A

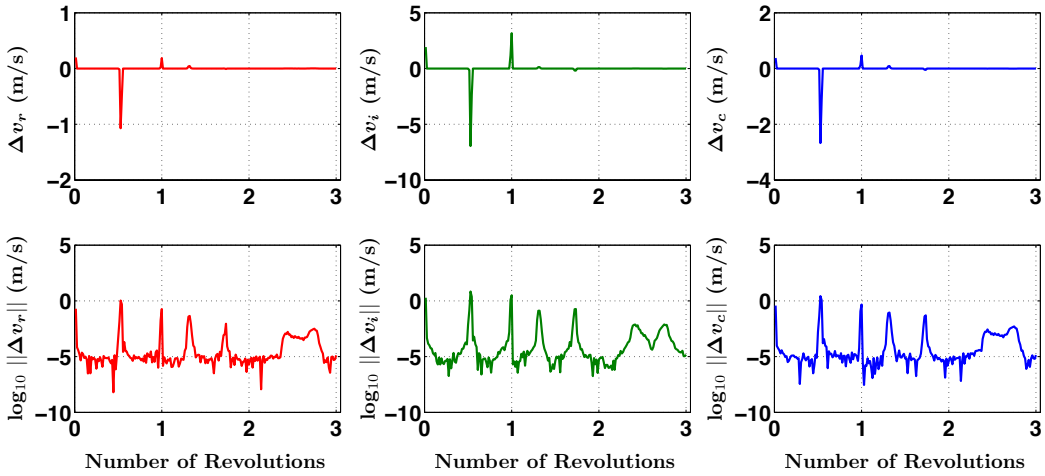

Figure 8: Fuel-optimal burn sequence determined by feedback control strategy for Example 3.

V Conclusion

An N-impulse feedback control law has been developed to mitigate specified errors in a set of nonsingular orbital element differences between a chief and deputy spacecraft in the geosynchronous regime. The linear mapping between these nonsingular element differences and the Cartesian Hill frame state of the deputy was derived, and the Gaussian variational equations for these nonsingular elements were developed to construct a basis for the presented feedback control methodology. Using this N-impulse strategy, a near-optimal burn sequence may be quickly determined to provide an estimate of appropriate initial conditions for more complex nonlinear optimization algorithms. By specifying impulses to occur every $f_{\Delta v}$ in true anomaly, this strategy "detects" fuel-optimal burn locations for general transfers in which the optimal burn locations are unknown, such that ideal initial conditions for a nonlinear optimizer seeking a two or three-burn solution are discerned.

References

[1] Schaub, H. and Alfriend, K. T., "Impulsive Feedback Control to Establish Specific Mean Orbit Elements of Spacecraft Formations," *Journal of Guidance, Navigation, and Control*, Vol. 24, No. 4, August 2001.

[2] Schaub, H., "Spacecraft Relative Orbit Geometry Description through Orbit Element Differences," *Proceedings of the 14th U.S. National Congress of Theoretical and Applied Mechanics*, June 2002.

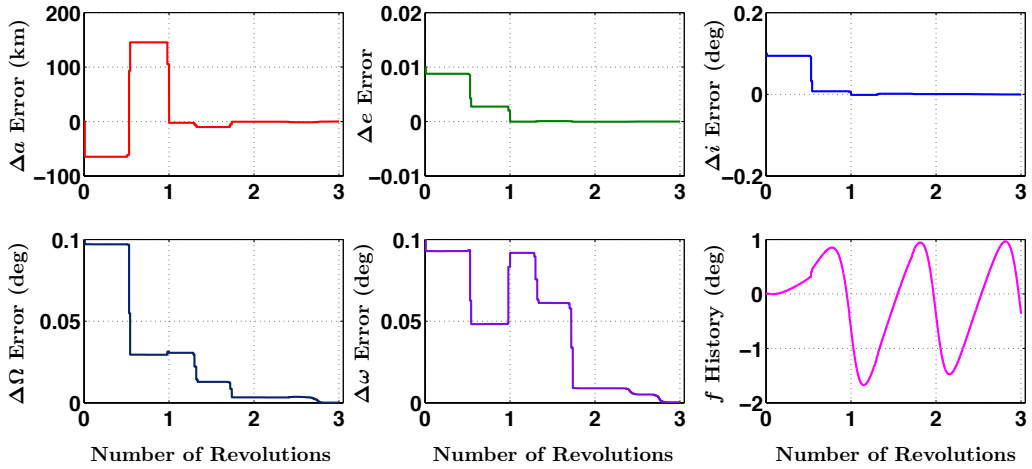

Figure 9: Error history of classical orbit elements during burn sequence execution for Example 3.

[3]Schaub, H., "Incorporating Secular Drifts into the Orbit Element Difference Description of Relative Orbits," *Proceedings of the 13th AAS/AIAA Space Flight Mechanics Meeting*, February 2003.

[4]Cougnet, C., Gerber, B., and Visentin, G., "On-Orbit Servicing System Architectures for GEO and MEO Constellations," *Proceedings of the 57th International Astronautical Congress*, International Astronautical Federation, October 2006.

[5]Alfriend, K. T., Lee, D., and Creamer, N., "Optimal Servicing of Geosynchronous Satellites," *Journal of Guidance, Control and Dynamics*, Vol. 29, No. 1, 2006, pp. 203–206.

[6]Shen, H. and Tsiotras, P., "Peer-to-Peer Refueling for Circular Satellite Constellations," *Journal of Guidance, Control and Dynamics*, Vol. 28, No. 6, 2005, pp. 1220–1230.

[7]Tombasco, J., *Orbit Estimation of Geosynchronous Objects via Ground-Based and Space-Based Optical Tracking*, Ph.D. thesis, University of Colorado at Boulder, 2011.

[8]Nacozy, P. and Dallas, S., "The Geopotential in Nonsingular Elements," *Celestial Mechanics*, Vol. 15, 1977, pp. 453–466.

[9]Broucke, R. A. and Cefola, P. J., "On the Equinoctial Orbit Elements," *Celestial Mechanics*, Vol. 5, 1972, pp. 303–310.

[10]Schaub, H. and Junkins, J. L., *Analytical Mechanics of Space Systems*, American Institute of Aeronautics and Astronautics, Inc., 2nd ed., 2009.

[11]Prussing, J. E. and Chiu, J.-H., "Optimal Multiple-Impulse Time-Fixed Rendezvous Between Circular Orbits," *Journal of Guidance, Control and Dynamics*, Vol. 9, No. 1, January 1986.

[12]Vadali, S. R., Schaub, H., and Alfriend, K. T., "Initial Conditions and Fuel-Optimal Control for Formation Flying Satellites," *Proceedings of the 1999 AIAA Guidance, Navigation and Control Conference*, August 1999.

[13]Shen, H. and Tsiotras, P., "Optimal Two-Impulse Rendezvous using Multiple-Revolution Lambert Solutions," *Journal of Guidance, Control and Dynamics*, Vol. 26, No. 1, January 2003.

[14]Smith, J. E., *Application of Optimization Techniques to the Design and Maintenance of Satellite Constellations*, Master's thesis, Massachusetts Institute of Technology, June 1999.

[15]Abdelkhalik, O. and Mortari, D., "N-Impulse Orbit Transfer using Genetic Algorithms," *Journal of Spacecraft and Rockets*, Vol. 44, 2007, pp. 456–459.

[16]Alfriend, K. T., Schaub, H., and Gim, D.-W., "Gravitational Perturbations, Nonlinearity and Circular Orbit Assumption Effects on Formation Flying Control Strategies," *2000 AAS Guidance and Control Conference Proceedings*, AAS/AIAA, February 2000.

[17]Curtis, H., *Orbital Mechanics for Engineering Students*, Elsevier Butterworth-Heinemann, 2005.